

# IV

## Publication IV

K. Yliniemi, P. Ebbinghaus, P. Keil, K. Kontturi, G. Grundmeier, Chemical composition and barrier properties of Ag nanoparticle-containing sol-gel films in oxidizing and reducing low-temperature plasmas, *Surf. Coat. Technol.* **201** (2007) 7865-7872.

© 2007 Elsevier Science

Reprinted with permission from Elsevier B.V.



# Chemical composition and barrier properties of Ag nanoparticle-containing sol–gel films in oxidizing and reducing low-temperature plasmas

Kirsi Yliniemi<sup>a</sup>, Petra Ebbinghaus<sup>b</sup>, Patrick Keil<sup>b,\*</sup>, Kyösti Kontturi<sup>a</sup>, Guido Grundmeier<sup>b,1</sup>

<sup>a</sup> *Laboratory of Physical Chemistry and Electrochemistry, Helsinki University of Technology, P.O. Box 6100, FI-02015 TKK, Finland*

<sup>b</sup> *Max-Planck-Institut für Eisenforschung GmbH, Max-Planck Str. 1, 40237 Düsseldorf, Germany*

Received 9 November 2006; accepted in revised form 14 March 2007

Available online 21 March 2007

## Abstract

Silver nanoparticle-containing silica sol–gel coatings were synthesised using tetraethylorthosilicate (TEOS), HNO<sub>3</sub> and AgNO<sub>3</sub> as the main precursors and 3-(2-aminoethylamino)propyl trimethoxysilane (DIAMO) as a stabiliser. The stability and the barrier properties of the coatings were studied by means of UV/Vis spectroscopy, FTIR reflection absorption spectroscopy (IRRAS), spectroscopic Ellipsometry and electrochemical impedance spectroscopy (EIS). Both the long-term stability and barrier properties of the coatings could be tailored by low-temperature O<sub>2</sub> and H<sub>2</sub>-plasma treatments. The oxidative plasma treatment enabled the change of the matrix from organic–inorganic to silica-like and the reductive treatment led to a reduction of the formed passive film on the Ag nanoparticles within the matrix. Thereby, based on the combination of sol–gel chemistry with subsequent plasma treatment new thin film functionalities can be achieved.

© 2007 Elsevier B.V. All rights reserved.

*PACS:* 82.35.Np, Nanoparticles in polymers; 81.07.-b, Nanoscale materials and structures: fabrication and characterization; 81.65.-b, Surface treatments

*Keywords:* Ag nanoparticles; Silica matrix; Barrier properties; Plasma

## 1. Introduction

Nanoparticles, especially Ag nanoparticles, encapsulated in silica-like or organosilicon films have been studied intensively over the last decade. The possible applications of such materials range from antibacterial to optical applications [1–7]. The interest in hygienic coatings has intensified recently, especially, as the awareness of the serious health risks [8,9] posed by harmful bacterial colonisation on surfaces within schools, kitchens and in particular hospitals increased.

Silver doped silica-like coatings can be easily prepared using tetraethyl orthosilicate (TEOS), AgNO<sub>3</sub> and HNO<sub>3</sub> as the main precursors [1–3] and it is known that the siloxane bridges (Si–O–Si) form the inorganic backbone of the coating if it is prepared using the sol–gel method [4]. Hydrolysis and

polymerization reactions of TEOS could be achieved in the presence of water by controlling the pH of the solution to a sufficient level [4]. Uniform TEOS coatings have been reported to be obtained after annealing at 60 °C–120 °C and the Ag nanoparticles are known to be formed inside the coating with thermal treatment up to 600 °C either in air [1,2] or in reducing atmospheres [3]. In addition to thermal treatments also UV curing of sol–gel films [10] and  $\gamma$ -radiation exposure of mesoporous silica immersed in Ag<sup>+</sup> ions containing bath [11,12] have been found to be successful methods for the preparation of embedded Ag nanoparticles and nanoclusters in the silica-like coatings. For UV curing the main precursors of the sol–gel film were 3-(glycidoxypropyl)-trimethoxy silane (GLYMO) and 3-(methacryloxypropyl)-trimethoxy silane (MEMO) rather than the TEOS used in this study [10].

The effects of heat treatment on the stability and the formation of Ag nanoparticles have been studied intensively in recent years. Mennig et al. [3] observed that after drying at 120 °C in air colloidal Ag was formed within the film matrix and that at higher temperatures (400–500 °C) in a reducing atmosphere (N<sub>2</sub>/H<sub>2</sub>)

\* Corresponding author. Tel.: +49 211 6792 548; fax: +49 211 6792 440.

E-mail address: [keil@mpie.de](mailto:keil@mpie.de) (P. Keil).

<sup>1</sup> Current address: Department of Technical and Macromolecular Chemistry University of Paderborn Warburgerstr. 100, 33098 Paderborn, Germany.

first  $\text{Ag}_x\text{O}_y$  forms but that it reduces again to pure Ag when the temperature is further increased to 500–600 °C. De et al. [1] have studied the films using FTIR and the results of the films on silicon wafer showed that  $\equiv\text{Si}-\text{O}-\text{Ag}$  networks with non-bridging oxygen (other than as  $\text{Si}-\text{OH}$  groups) were formed after drying at 60 °C in air, whilst the formation of Ag nanoclusters was observed after a heat treatment in the temperature range of 300 to 600 °C. According to De et al. some silver clusters of 15 nm were already formed at low temperature on the surface of the porous network but a majority of the silver is either in atomic or ionic form [1].

Jeon et al. [2] were able to prepare uniform and transparent films after annealing at 100 °C in air but only after the thermal treatment in air with a temperature range of between 200 °C and 600 °C did the films turned yellow and Ag nanoparticles form. Below 500 °C the treated samples were unstable in natural light as the colour changed from yellow to dark yellow after a couple of days and this was explained by the incomplete trapping of  $\text{Ag}^+$  ions in the silica matrix. Shibata et al. [13] prepared films by annealing the samples in  $\text{N}_2$  flow and the stability was studied by irradiating with UV light. It was observed that the absorbance of the samples which were heat treated below 500 °C decreased whilst the films heat treated at 800 °C were found to be stable even after 20 h of irradiation.

The type of stabiliser used within coating preparation also has a significant effect on the size and properties of the resulting particles and several amino silanes have been used to reduce  $\text{AgNO}_3$  in ethanol to achieve Ag nanoparticles [14]. Some of these amino silanes have also been found to be suitable stabilisers for Ag nanoparticles in sol–gel coatings [3].

Despite the huge amount of synthesis research in the field, the detailed chemistry between the silicate coating and Ag nanoparticles is still not completely understood. Furthermore, the barrier properties – which will be of critical importance for the future practical applications – have not been studied extensively.

The work presented here introduces a simple sol–gel synthesis for preparing amino stabilised Ag nanoparticles embedded in inorganic–organic hybrid films. The properties of the film matrix and the incorporated Ag nanoparticles were modified by means of low-temperature  $\text{H}_2$  and  $\text{O}_2$ -plasma treatments. The  $\text{O}_2$ -plasma treatment was used for the calcination of the  $\text{SiO}_2$  matrix and the subsequent  $\text{H}_2$ -plasma treatment was applied to reduce the passive silver oxide film on the Ag nanoparticles formed during the  $\text{O}_2$ -plasma treatment. The stability of the films was studied by means of UV/Vis Spectroscopy and FT-IRRAS (FTIR reflection absorption spectroscopy). Moreover, the changes in barrier properties of the coatings due to plasma treatments and Ag nanoparticles were studied with electrochemical impedance spectroscopy (EIS). Hence, the effects due to the silica matrix and Ag nanoparticles could be distinguished, whilst the effect of the interaction between the Ag particles and the surrounding matrix on the barrier properties of the composite film could also be studied.

## 2. Experimental

The precursors used to produce Ag nanoparticle-containing sol–gel coatings included tetraethyl orthosilicate (TEOS,

Merck, 98%),  $\text{HNO}_3$  (Merck, 65%), ethanol (Merck, p.a.), methanol (Merck, p.a.), 3-(2-aminoethylamino)propyl trimethoxysilane (DIAMO, ABCR, 96%) and  $\text{AgNO}_3$  (Merck, p.a.), respectively. Firstly,  $\text{AgNO}_3$ , with a molar ratio of  $\text{AgNO}_3$ :DIAMO of 1:1, was dissolved in a solution containing methanol and DIAMO. The sol–gel solution containing 10.12 ml TEOS, 10.60 ml ethanol and 1.23 ml  $\text{HNO}_3$  (0.1 M, prepared with MQ-water) was added to the solution of methanol+DIAMO+ $\text{AgNO}_3$  resulting in the molar ratio of Ag:Si of about 1:30 and the solution was further stirred for 15 min. During the whole preparation procedure the solutions containing  $\text{Ag}^+$  ions were protected from light by using an aluminum foil.

Samples with a size of  $2 \times 2 \text{ cm}^2$  were either prepared from polished stainless steel (ThyssenKrupp Steel) for IR and EIS measurements, glass laboratory slides (Menzel GmbH) for UV/Vis spectroscopy or polished p-type Si (100) wafers (Si-Mat Germany) for spectroscopic Ellipsometry measurements. Prior to film deposition, the stainless steel samples were solvent cleaned in ultrasonic bath of tetrahydrofuran, 2-propanol and ethanol (all Merck, p.a.), for 15 min in each solution, whilst glass slides and the Si-wafers were alkaline cleaned in a solution of ammonia ( $\text{NH}_3$ , Merck, 65%) and hydrogen peroxide ( $\text{H}_2\text{O}_2$ , Merck, 35%), with a volume ratio of 1:1 at 80 °C.

The cleaned samples were dipped into the freshly prepared mixture of the sol–gel solution and the  $\text{AgNO}_3$ +DIAMO+ methanol solution. Dipping was carried out by means of a dip-coater with a speed of 2 mm/s. After film formation the samples were dried at 120 °C in air for 30 min. The oxygen plasma treatment was performed in a plasma chamber with a linear microwave source (Roth and Rau, Germany) at a frequency of 2.46 GHz. Prior to the plasma treatment the process chamber was evacuated down to a pressure of 0.02 mbar and afterwards flushed three times with argon. The samples were plasma treated for 10 min at an RF-power of 300 W in an oxygen atmosphere of 0.2 mbar and an oxygen flux of 80 sccm. The hydrogen plasma treatment was done by means of an audio frequency plasma process. Prior to the plasma treatment the process chamber was evacuated down to a pressure of  $3 \cdot 10^{-3}$  mbar. Afterwards, the samples were plasma treated for 10 min at 4 kHz, in a hydrogen atmosphere of 0.3 mbar and a process gas flux of 5.2 ml/min.

The resulting Ag-containing sol–gel coatings were studied either by FT-IRRAS at an 80° angle of incidence (Varian, FTS 3000), spectroscopic Ellipsometry (SE 800, Sentech, Germany) or UV/VIS (Perkin-Elmer, Lambda 800) before and after the plasma treatments. UV/Vis spectra were measured in transmission mode using the glass samples, with a wavelength range of 900 nm to 260 nm. The spectroscopic Ellipsometry measurements were done in the wavelength range of 300–800 nm at three different incident angles of 50°, 60° and 70°. The mass spectrometry measurements were performed by using a time of flight secondary ion mass spectrometry (ToF-SIMS) TRIFT II System (Physical Electronics). The primary  $\text{Ga}^+$  ion beam was accelerated by a 15 kV voltage and had an intensity of 600 pA.

The barrier properties of the coatings both before and after plasma treatments and additionally in the absence of Ag

nanoparticles were studied by means of electrochemical impedance spectroscopy (EIS) using a Gamry FAS 2 Femtostat. The EIS measurements were performed in a standard three electrode cell in a borate buffer solution at room temperature – consisting of 0.2 M  $\text{H}_3\text{BO}_3$ , 0.05 M  $\text{Na}_2\text{SO}_4$ , 0.05 M  $\text{Na}_2\text{B}_4\text{O}_7 \cdot 10\text{H}_2\text{O}$  (all Merck, p.a.) with a pH=8.4 – under potentiostatic control at open circuit potential using a Ag/AgCl/3 M KCl reference electrode and a gold wire as a counter electrode. The applied frequencies ranged from 200 kHz to 0.1 Hz and the exposed area of a sample used as a working electrode was kept constant at  $0.75 \text{ cm}^2$ .

### 3. Results and discussion

#### 3.1. Optical spectroscopy

Fig. 1 shows the UV/Vis spectra of Ag nanoparticles containing an inorganic–organic sol–gel film on a glass substrate as a function of time of exposure to light and laboratory air. The increment in the figure shows the change in the maximum absorbance and the position of the surface plasmon resonance (SPR) peak of the silver nanoparticles as a function of time. The freshly prepared coating showed a SPR peak centred at 415 nm indicating the presence of Ag nanoparticles in the coating as the surface plasmon peak of silver has been reported to be around 400–430 nm in silica-like matrices [7,11,15]. However, despite the formation of Ag nanoparticles it is still possible that a reasonable amount of silver is dissolved into the organic matrix either in atomic or ionic form, similar to the observations of De et al. [1]. After 1 h exposure the maximum absorbance of the peak decreased from 0.087 to 0.081 without any further changes in the peak. After 24 h of exposure the centre of the peak shifted to 423 nm and the maximum absorbance decreased even further to 0.071. In addition, the shape of the peak broadened significantly and the absorbance level increased in the wavelength range between 600 nm and 800 nm.

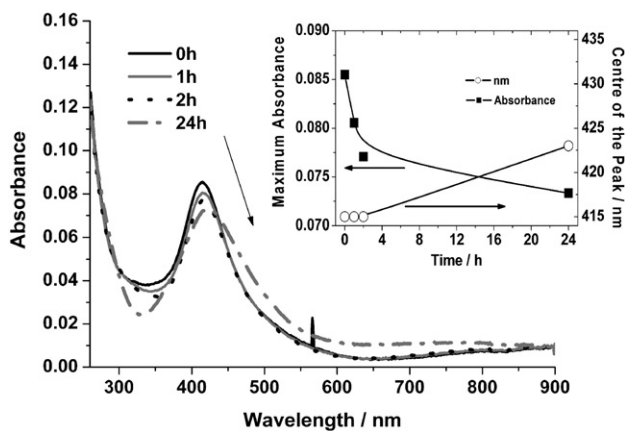


Fig. 1. UV/Vis spectra of Ag nanoparticle-containing sol–gel film on glass substrate as a function of time when exposed to natural light and laboratory air. The increment in the figure shows the centre of the peak (right axis) and the maximum absorbance of the peak (left axis) as a function of time; N.B. the solid lines connecting the measured points are only there to improve clarity.

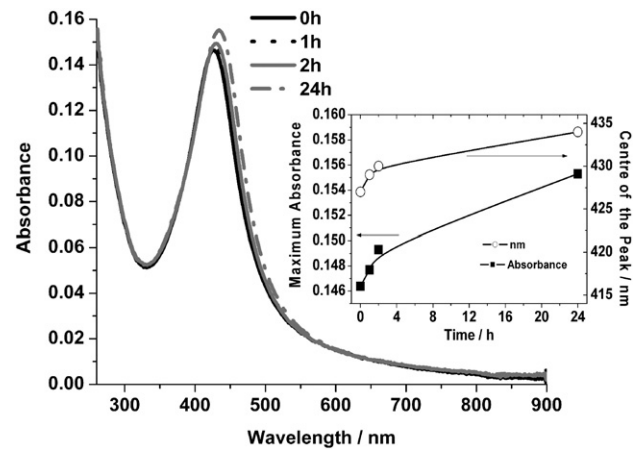


Fig. 2. UV/Vis spectra of Ag nanoparticle-containing sol–gel film on glass substrate after 10 min  $\text{O}_2$ -plasma treatment as a function of time when exposed to the natural light and laboratory air. The increment in the figure shows the centre of the peak (right axis) and the maximum absorbance of the peak (left axis) as a function of time; N.B. the solid lines connecting the measured points are only there to improve clarity.

These observations are similar to those reported in literature. Mennig et al. [3] prepared films using DIAMO as a stabiliser and observed that after the heating at  $120^\circ\text{C}$  in air almost all Ag is actually in the form of colloidal Ag. Li et al. [16] also suggested that already during the drying process silver colloids are formed and that the decrease of the absorbance and the diminishing yellow colour of the film with increasing heating temperature in air are due to oxidation of silver particles [16]. In contrast, however, Ritzer et al. [17] attributed the bleaching of Ag-containing sol–gel films as a function of time and temperature to the agglomeration of silver particles [17].

The shift in the peak position during the exposure in Fig. 1 may also be explained by a matrix-effect. Ag clusters and the excess of  $\text{Ag}^+$  ions may react with the amino and silanol groups of the matrix, similar to the case Jeon et al. described [2]. The decrease in maximum absorbance of the peak could be then

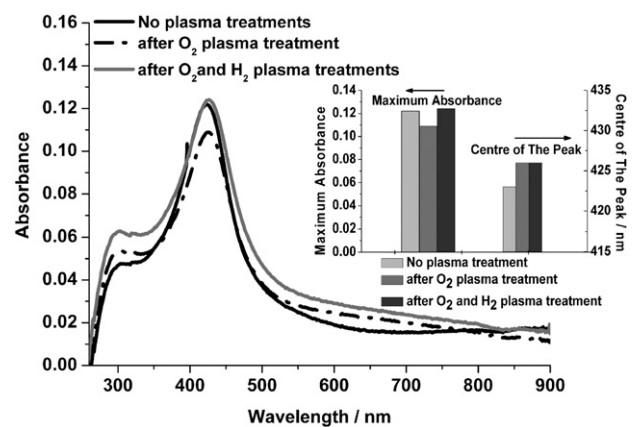


Fig. 3. UV/Vis spectra of Ag nanoparticle-containing sol–gel films on glass substrate before plasma treatment, after 10 min of  $\text{O}_2$ -plasma treatment and finally after 10 min of  $\text{O}_2$ -plasma treatment+10 min  $\text{H}_2$ -plasma treatment. The increment in the figure shows the centre of the peak (right axis) and the maximum absorbance of the peak (left axis) as a function of plasma treatments.

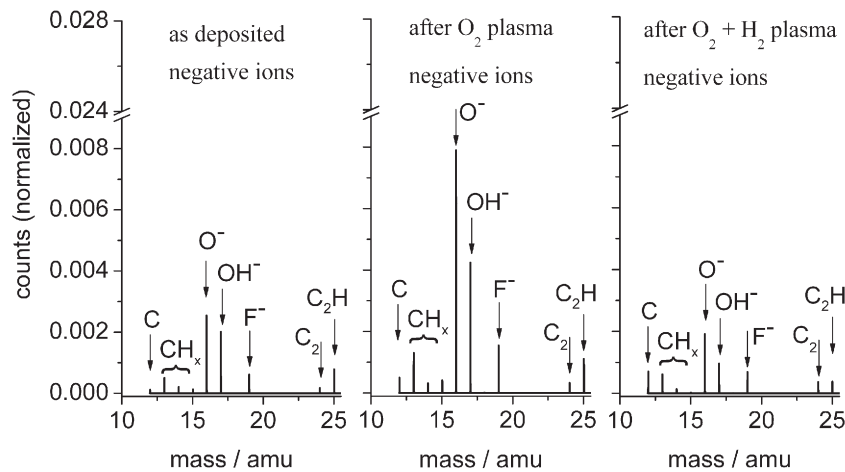


Fig. 4. ToF-SIMS measurements of unmodified and plasma treated thin Ag films (as indicated).

related to the oxidation of the nanoparticles similar to that seen by Li et al. [16]. Weibing et al. [18] studied the formation of  $\text{Ag}_2\text{O}$  as a passivating layer on silver nanoparticles in porous silica matrix by atmospheric oxygen and according to their observations silver oxide can form on the surface of silver nanoparticles in humid air (60% r.h.) within less than a week.

The effects of the passivation of the nanoparticle surface and the change in the matrix chemistry can be further studied by the calcination of the thin film coating in low-temperature  $\text{O}_2$  plasmas as the calcination leads to conversion of the inorganic–organic matrix into a silica-like network. The surface plasmon resonance of Ag nanoparticle-containing sol–gel films after  $\text{O}_2$ -plasma treatment was studied with UV/Vis (Fig. 2) and the chemical conversion of the film matrix was analysed via FT-IRRAS (see Fig. 5).

The UV–Vis spectra after  $\text{O}_2$ -plasma treatment show that the position of the peak maximum is shifted from 415 to 427 nm.

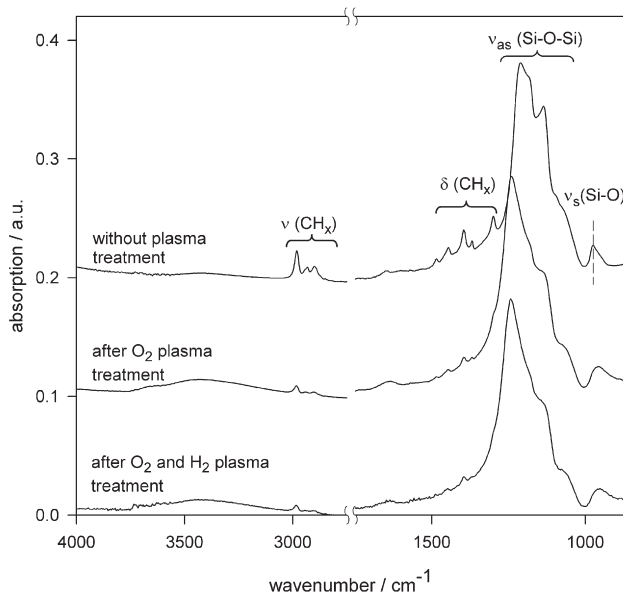


Fig. 5. FTIR spectra of Ag nanoparticles containing  $\text{SiO}_2$ -like film on stainless steel (as indicated). The spectra are vertically displaced by 0.1 U.

Moreover, the peak width at half height is only slightly broadened. The effect of air and light on the Ag/ $\text{SiO}_2$  coating after the  $\text{O}_2$ -plasma treatment (Fig. 2) is less prominent than without the plasma treatment (Fig. 1). The maximum absorbance is almost unchanged during the first 2 h and after 24 h exposure the absorbance has even slightly been increased from 0.146 (at 0 h) to 0.155 (at 24 h). Furthermore, the shape of the peak remains similar during the whole exposure time and no increase in the absorption in the wavelength range 600–800 nm was observed. However, the position of the peak is shifted from 427 nm to 434 nm during the first 24 h (Fig. 2) and is similar to the changes without  $\text{O}_2$ -plasma treatment observed in Fig. 1.

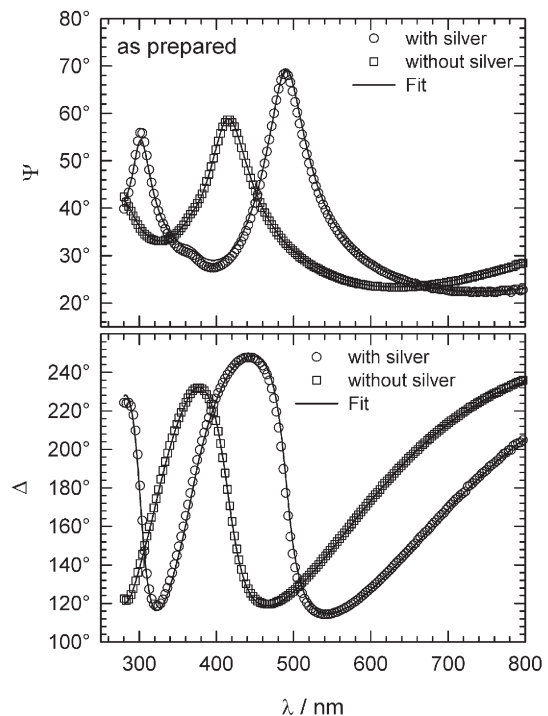


Fig. 6. Variation of  $\Psi$  and  $\Delta$  with the wavelength at the incident angle of  $60^\circ$  for the sol–gel film coatings on Si substrate without plasma treatment (symbols: experimental data, lines: fit result).

Table 1

Optical parameters, thickness and Ag volume fraction determined by fitting ellipsometric data using the Cauchy and Maxwell–Garnett effective medium models

	$d/\text{nm}$	$f$	$n_0$	$n_1/\text{nm}^2$
Sol–gel coating without Ag nanoparticles				
°As prepared	268.5		1.417	41.2
°After O <sub>2</sub> -plasma treatment	204.5		1.406	34.5
°After O <sub>2</sub> and H <sub>2</sub> -plasma treatment	192.5		1.410	39.9
Sol–gel coating with Ag nanoparticles				
°As prepared	315.5	0.006		
°After O <sub>2</sub> -plasma treatment	211.9	0.008		
°After O <sub>2</sub> and H <sub>2</sub> -plasma treatment	201.0	0.008		

The UV/Vis spectra of a sample prior to the plasma treatment, with 10 min O<sub>2</sub>-plasma treatment and with both 10 min O<sub>2</sub> and 10 min H<sub>2</sub>-plasma treatments are compared in Fig. 3. The peak maximum shows a red shift after the oxygen plasma.

However, a significant decrease in the peak height and a broadening of the peak are observed after the 10 min O<sub>2</sub>-plasma treatment. The original absorbance and peak width are observed after the H<sub>2</sub>-plasma treatment. It is convincing that an oxidation of the Ag-nanoparticle surface takes place during the O<sub>2</sub>-plasma treatment resulting in the formation of an Ag<sub>2</sub>O shell on the

surface of the Ag nanoparticles. During the H<sub>2</sub>-plasma treatment, the passive film is once again reduced. This assumption is assisted by time of flight secondary ion mass spectroscopy (ToF-SIMS) measurements of evaporated silver films presented in Fig. 4 which show a significantly increased amount of oxygen at the surface after the oxygen plasma treatment. Thus, the O<sub>2</sub>-plasma treatment leads to an oxide formation on the Ag surface and a reduction of the Ag surface after the respective hydrogen plasma treatment can be achieved.

The FT-IRRAS spectra of a sample after different treatments (Fig. 5) show that calcination of sol–gel films occurs in the film during the O<sub>2</sub>-plasma treatment. The spectrum of the film prior to the plasma treatments clearly shows peaks attributable to both the organic functionalities of the precursor molecules (CH<sub>x</sub>) and inorganic groups (Si–O–Si) in the film [19].

Oxygen plasma treatment leads to a partial diminishing of the precursor peaks. Moreover, the asymmetric stretching peak of the Si–O–Si is shifted to higher wavenumbers indicating an increase in the network density and proving the partial calcination process to a silica-like film.

The increase in the peak intensity between 3300 and 3400 cm<sup>-1</sup> is assigned to the increase in hydrogen bonded silanol groups and adsorbed hydrogen bonded water molecules, whereas the hydrogen plasma treatment does not show any further changes in the chemical composition of the film.

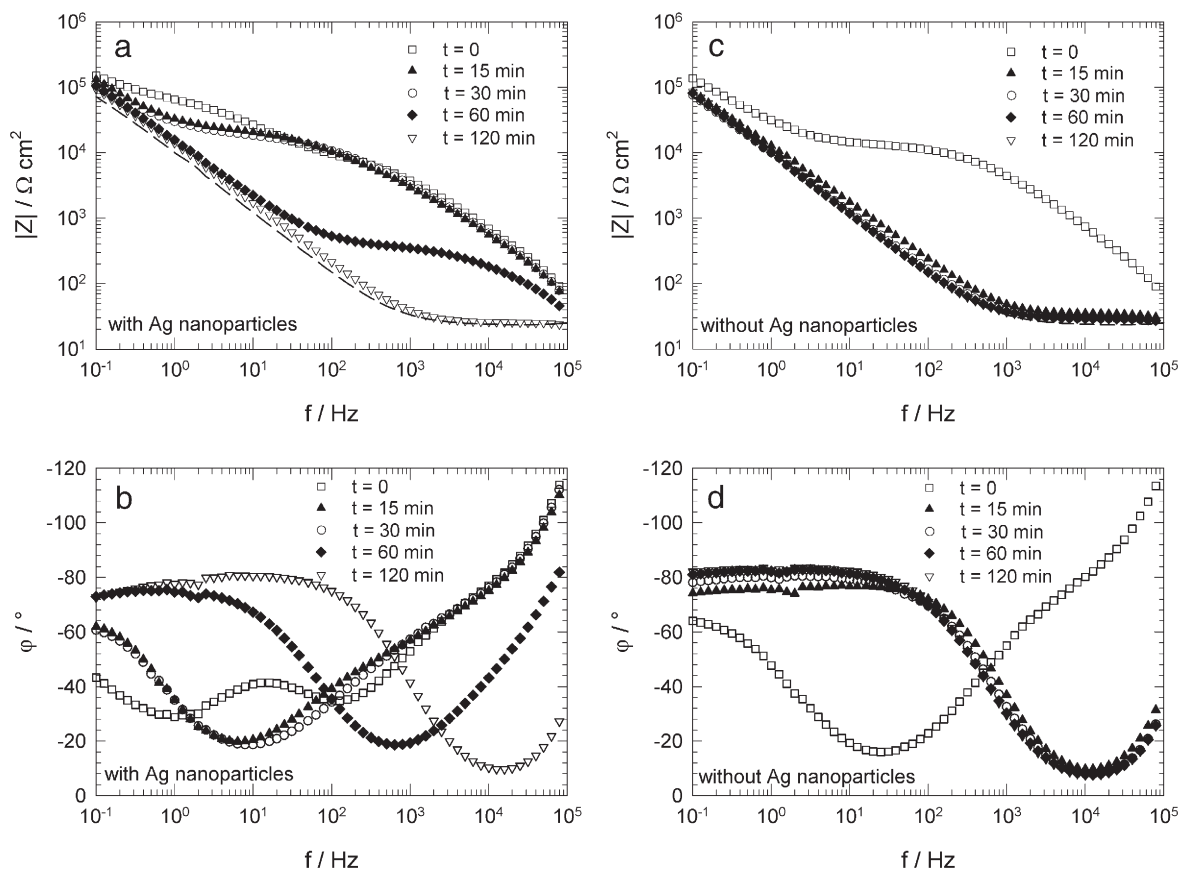


Fig. 7. Bode plots obtained for the of the sol–gel films coating with Ag nanoparticles (a, b) and without Ag nanoparticles (c, d) on stainless steel as a function of time during the exposure in borate buffer solution. The modulus of the impedance obtained for the uncoated stainless steel substrate after 120 min of exposure to the borate buffer is indicated by the dashed lines.

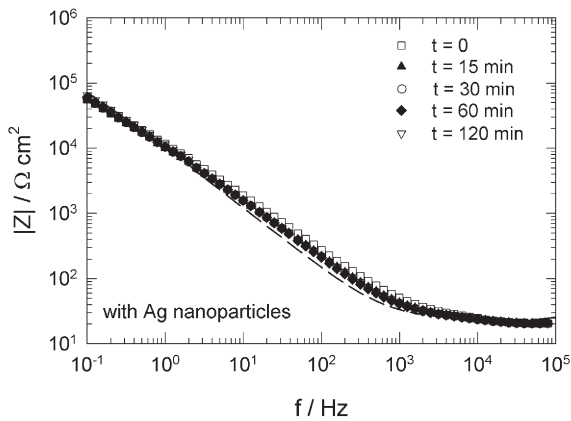


Fig. 8. Modulus of the impedance obtained for the of the sol-gel film coating with Ag nanoparticles on stainless steel after 10 min of  $O_2$ -plasma treatment as a function of time during the exposure in borate buffer solution. The modulus of the impedance obtained for the uncoated stainless steel substrate after 120 min of exposure to the borate buffer is indicated by the dashed line.

The combined evaluation of the UV/Vis and FT-IRRAS data indicates that the decrease in SPR peak height and broadening of the peak after oxygen plasma is related to the oxidation of the Ag-nanoparticle surface rather than to the chemical change of the surrounding matrix.

For the spectroscopic Ellipsometry measurements the same sol-gel film with embedded Ag was investigated directly after

film preparation (no plasma treatment) and after the following plasma treatment processes. The same procedure was applied to a reference sol-gel coating without any nanoparticles.

In order to determine the information from ellipsometric spectra a model describing the structure of the sample and its optical response to the ellipsometric quantities  $\Psi$  and  $\Delta$  is usually applied. Thereby  $\Psi$  is defined as  $\tan \Psi = |R^p|/|R^s|$ , where  $R^p$  and  $R^s$  are the total reflection coefficient, i.e. the ratio of the amplitude of the outgoing resultant wave to the amplitude of the incoming wave for the p-waves and s-waves and  $\Delta$  is defined as  $\Delta = \delta_1 - \delta_2$ , where  $\delta_1$  and  $\delta_2$  are the phase difference between the p-wave and the s-wave before the reflection and after the reflection.

In Fig. 6 the ellipsometric spectra for an incident angle of  $60^\circ$  of the the sol-gel films with and without Ag nanoparticles are shown exemplarily. Due to the interference of the light reflected at the film surface with the one reflected at the film/substrate interface one can see oscillation peaks in the spectra. In order to analyse the experimental data of the sol-gel films without Ag a model consisting of a layer having a Cauchy dispersion relation [20] and a Si substrate was employed. The Cauchy dispersion relation  $n(\lambda) = n_0 + n_1/\lambda^2$  accurately describes the refractive index of transparent materials like  $SiO_2$ . The model parameters and the film thickness  $d$  were acquired by fitting (e.g. by minimizing the mean square error) of the structural model to the experimental spectra.

Whilst the thickness of the films without embedded silver was determined using the Cauchy model, an effective medium

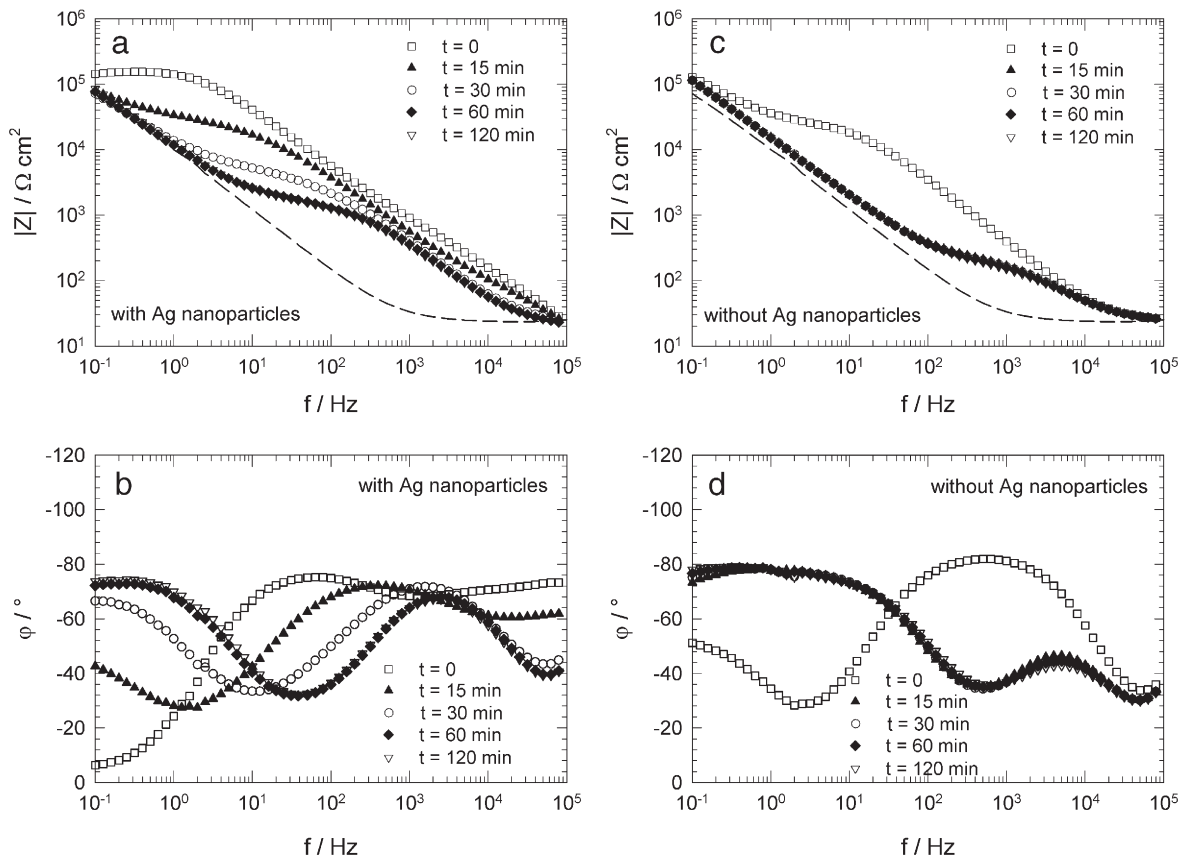


Fig. 9. Bode plots obtained for the  $SiO_2$ -like films with Ag nanoparticles (a, b) and without Ag nanoparticles (c, d) on stainless steel after 10 min of  $O_2$  and 10 min of  $H_2$ -plasma treatment as a function of time during the exposure in borate buffer solution. The modulus of the impedance obtained for the uncoated stainless steel substrate after 120 min of exposure to the borate buffer is indicated by the dashed lines.

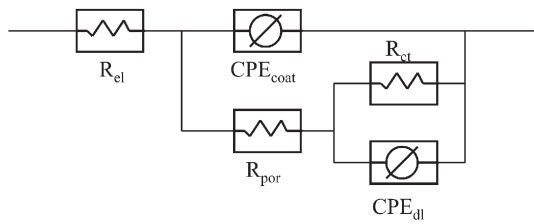


Fig. 10. General equivalent circuit used for numerical fitting of the impedance spectra obtained for the sol–gel coated stainless steel;  $R_{el}$  = resistance of the electrolyte,  $R_{por}$  = resistance of the pores,  $R_{ct}$  = charge transfer resistance,  $CPE_{coat}$  = non-ideal capacitor of the coating,  $CPE_{dl}$  = non-ideal capacitor of the electrode double layer.

approximation must be applied in order to determine the thickness of the films with embedded silver. In the present case the Maxwell–Garnett effective medium approximation [20] was used. This model assumes spherical inclusions of one medium (Ag) embedded in a host material ( $SiO_2$ -like matrix). Considering the complex index of refraction of the inclusion  $n_i$ , the host medium  $n_h$  and the volume fraction of the inclusion  $f$  one can describe the index of refraction of effective medium  $n_e$  as  $(n_e^2 - n_h^2)/(n_e^2 + 2n_h^2) = f \cdot (n_i^2 + n_h^2)/(n_i^2 + 2n_h^2)$ . In order to determine the film thicknesses and the volume fraction of the inclusion the Maxwell–Garnett approximation in combination with Cauchy dispersion relation for the host medium (acquired from the measurement without embedded Ag) and Drude–Lorentz oscillator model for silver was applied to fit the experimental results [20]. The determined values from the measurements at three different incident angles of  $50^\circ$ ,  $60^\circ$  and  $70^\circ$  of the sol–gel coatings are summarised in Table 1. As can be seen in Fig. 6 the experimental results are well-reproduced by these parameters and the applied models.

The spectroscopic Ellipsometry measurements reveal that due to the incorporation of Ag the coating with Ag nanoparticles exhibits an approximately 45 nm increased film thickness in comparison to the film without nanoparticles. Furthermore, the oxygen plasma treatment leads to a significant reduction of the film thickness due to the calcination process resulting in similar values for the coatings. In agreement with the FTIR results the subsequent hydrogen plasma only shows a minor reduction of the

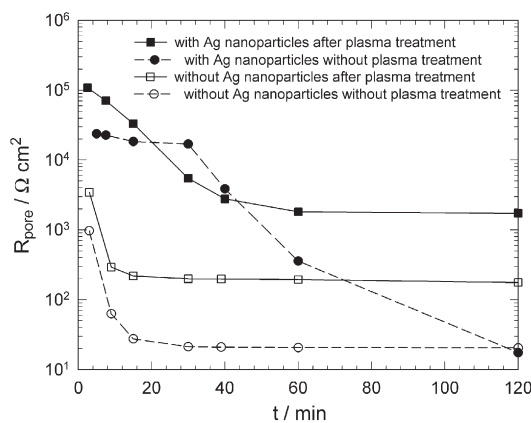


Fig. 11. Evolution of the pore resistance of the sol–gel coatings during immersion in borate buffer solution (pH=8.4). N.B. the lines connecting the measured points are only there to improve clarity.

film thickness indicating the absence of further changes in the chemical composition of the host material.

### 3.2. Electrochemical analysis

The barrier properties of the sol–gel coatings with and without silver nanoparticles were investigated by means of electrochemical impedance spectroscopy (EIS) as a function of exposure time in borate buffer solution. For the EIS measurements all sol–gel films with Ag nanoparticles (no plasma treatment,  $O_2$ -plasma treatment,  $O_2 + H_2$ -plasma treatment) were dip-coated simultaneously to create as identical samples as possible. The same procedure was applied to produce a reference sol–gel coating without any nanoparticles. After the EIS measurements all samples were analysed by means of FT-IRRAS to prove that the film thickness values were really comparable and that the changes in the impedance spectra could be assigned to structural changes within the films. As shown by Cui and Takoudis [21] the film thickness of  $SiO_2$ -like films can be correlated with the height of the absorption peak of the Si–O asymmetrical stretching and Si–O–Si stretching vibrations in IR spectra.

The Bode plots obtained from the sol–gel films with and without Ag nanoparticles during the exposure to the borate buffer solution are presented in Fig. 7(a,b) and (c,d), respectively. After 15 min of exposure the spectra in both cases reveal the presence of two well-defined time constants. The time constant at higher frequencies ( $f > 10^3$  Hz) can be assigned to the penetration of solution into the sol–gel film, which leads to a change in the film capacitance whilst the time constant at frequencies lower than 1 Hz can be assigned to the pore resistance. Comparing the modulus of the impedance of the coating with Ag nanoparticles (Fig. 7a) with the film without nanoparticles (Fig. 7c) it is apparent that the pore resistance of the coating with nanoparticles is significantly higher. The barrier properties of the coating without nanoparticles decrease dramatically within the first 15 min of exposure and the related capacitance decreases to the characteristics values of pure

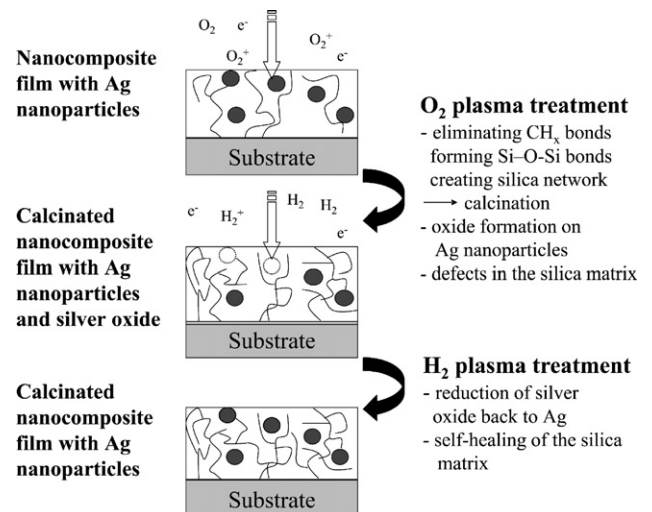


Fig. 12. Schematic model of the changes to the coating after treatment first with 10 min of  $O_2$ -plasma treatment and then with 10 min of  $H_2$ -plasma treatment.

stainless steel. For the film with nanoparticles the strong decrease of the impedance is observed only after 2 h. After the EIS investigation the coated specimens were dehumidified and it was proven by FT-IRRAS spectroscopy that the films were still intact and adhering to the substrate surface after the immersion in the electrolyte.

Fig. 8 presents the impedance spectra of the sol–gel films with Ag nanoparticles after 10 min of O<sub>2</sub>-plasma treatment. The impedance spectra of O<sub>2</sub>-plasma treated nanocomposite film show the characteristic behavior of stainless steel already within the first 2 min of immersion. Due to the oxygen plasma treatment the wettability of the sol–gel film is considerably increased, resulting in a more hydrophilic coating compared to the film without any plasma treatment, this allows the electrolyte to penetrate the coating almost instantaneously due to capillary force induced convection through the pinholes.

In Fig. 9 the Bode plots of the films after 10 min of O<sub>2</sub> and 10 min of H<sub>2</sub>-plasma treatment, with and without Ag nanoparticles, are shown. In comparison to Fig. 7, the pore resistance values of the films with nanoparticles (left side) and the films without nanoparticles (right side) were clearly increased after treatment with the hydrogen plasma. This leads to the conclusion that during the H<sub>2</sub>-plasma treatment the barrier properties are once more increased due to the reduction of the newly created Ag-oxide shell (from the O<sub>2</sub>-plasma treatment) in agreement with the results of the UV/Vis spectra.

The impedance spectra were fitted according to a general equivalent circuit used to evaluate the pore resistance. Instead of an ideal capacitor a constant phase elements (CPE) was used to take into account a certain degree of inhomogeneity of the thin nanocomposite films. Fig. 10 shows the equivalent circuit used for the quantitative data analysis. In this equivalent circuit,  $R_{el}$  represents the electrolyte resistance,  $CPE_{coat}$  is related to the non-ideal capacitance of the sol–gel coating,  $R_{por}$  is the pore resistance of the sol–gel coating,  $CPE_{dl}$  is related to the non-ideal capacitance of the double layer of the bare steel and  $R_{ct}$  is the charge transfer resistance.

The evolution of the pore resistance for sol–gel coatings presented in Figs. 7 and 9 during the exposure to the borate buffer is shown in Fig. 11. Initially, the pore resistances of films with nanoparticles are about one order of magnitude higher than the corresponding values of films without nanoparticles. The higher resistance of the nanoparticle-containing sol–gel films could be due to the lower concentration of the conductive pathways through the coating. After a few minutes of exposure, the resistance started to decrease as a function of time for all films. However, the pore resistances of the films with Ag nanoparticles and without any plasma treatment were almost constant for the first 40 min of exposure before a rapid decrease was observed. After 120 min of exposure the resistance values of the sol–gel film with nanoparticles and after the combined O<sub>2</sub> and H<sub>2</sub>-plasma treatment reached a stable value that was more than one magnitude larger than that seen for all other films.

The schematic in Fig. 12 summarises the modifications of the sol–gel film that take place during oxygen and hydrogen plasma treatments.

#### 4. Conclusions

Silver nanoparticle-containing silica sol–gel coatings were synthesised using tetraethylorthosilicate (TEOS), HNO<sub>3</sub> and AgNO<sub>3</sub> as the main precursors and 3-(2-aminoethylamino) propyl trimethoxysilane (DIAMO) as a stabiliser. Both the long-term stability and barrier properties of the coatings could be tailored by low-temperature O<sub>2</sub> and H<sub>2</sub>-plasma treatments. The O<sub>2</sub>-plasma induced partial calcination of the film is accompanied by an oxide formation on the Ag-nanoparticle surface. Reduction of Ag-nanoparticle surface during the H<sub>2</sub>-plasma treatment is achieved. The combined oxygen and hydrogen plasma treatment leads to films that are more stable under atmospheric conditions and show increased barrier properties. The presence of Ag nanoparticles in the matrix leads to an increase in the impedance for all film compositions.

#### Acknowledgements

TEKES (Finnish Funding Agency for Technology and Innovation) and Fortum Foundation are acknowledged for their financial support of this research and enabling Kirsii Yliniemi's visit in Max-Planck-Institut für Eisenforschung GmbH. The Max-Planck-Institut für Eisenforschung GmbH acknowledges the financial support within the framework of the DECOBIOF Project of the Research Fund Coal and Steel of the European Community (Contact RFSR-CT-2005-00024).

#### References

- [1] G. De, A. Licciucilli, C. Massaro, L. Tapfer, M. Catalano, G. Battaglin, C. Meneghini, P. Mazzoldi, *J. Non-Cryst. Solids* 194 (1996) 225.
- [2] H.-J. Jeon, S.-C. Yi, S.-G. Oh, *Biomaterials* 24 (2003) 4921.
- [3] M. Mennig, M. Schmitt, H. Schmidt, *J. Sol–Gel Sci. Technol.* 8 (1997) 1035.
- [4] F.H. Scholes, S.A. Furman, D. Lau, C.J. Rossouw, T.J. Davis, *J. Non-Cryst. Solids* 347 (2004) 93.
- [5] F. Gonella, *Nucl. Instrum. Methods B* 166–167 (2000) 831.
- [6] P.D. Townsend, D.E. Hole, *Vacuum* 63 (2001) 641.
- [7] D.K. Sarkar, F. Cloutier, M.A. El Khakani, *J. Appl. Phys.* 97 (2005) 084302-1.
- [8] J.W. Costerton, P.S. Stewart, E.P. Greenberg, *Science* 284 (1999) 1318.
- [9] N. Fishman, *Am. J. Infect. Control* 34 (2006) S55.
- [10] G. De, D. Kundu, *J. Non-Cryst. Solids* 228 (2001) 221.
- [11] V. Hornebecq, M. Antonietti, T. Cardinal, M. Treguer-Delapierre, *Chem. Mater.* 15 (2003) 1993.
- [12] A.L. Pan, H.G. Zheng, Z.P. Yang, F.X. Liu, Z.J. Ding, Y.T. Qian, *Mater. Res. Bull.* 38 (2003) 789.
- [13] S. Shibata, K. Miyajima, Y. Kimura, T. Yano, *J. Sol–Gel Sci. Technol.* 31 (2004) 123.
- [14] A. Frattini, N. Pellegrini, D. Nicastro, O. De Sancti, *Mater. Chem. Phys.* 94 (2005) 148.
- [15] C. Weibing, Z. Lide, *J. Phys., Condens. Matter* 9 (1997) 7257.
- [16] W. Li, S. Seal, E. Megan, J. Ramsdell, K. Scammon, G. Lelong, L. Lachal, K.A. Richardson, *J. Appl. Phys.* 93 (2003) 9553.
- [17] B. Ritzer, M.A. Villegas, J.M. Fernández Navarro, *J. Sol–Gel Sci. Technol.* 8 (1997) 917.
- [18] C. Weibing, T. Ming, Z. Lide, *J. Phys., Condens. Matter* 9 (1997) 1995.
- [19] J.-J. Kim, H.-H. Park, S.-H. Hyun, *Thin Solid Films* 377–378 (2005) 525.
- [20] H.G. Tompkins, W.A. McGahan, *Spectroscopic Ellipsometry and Reflectometry*, John Wiley & Sons, 1999.
- [21] Z. Cui, C.G. Takoudis, *J. Appl. Phys.* 89 (2001) 5170.